Characterization of Liquid Flow in the Spinning Cloth Disc Reactor: Residence Time Distribution, Visual Study and Modeling

Xudong Feng[1], Darrell Alec Patterson[2], Murat Balaban[1]

and Emma Anna Carolina Emanuelsson[2]*

[1] Department of Chemical and Materials Engineering, University of Auckland,

Private Bag 92019, Auckland Mail Centre, Auckland, 1142, New Zealand.

[2] Department of Chemical Engineering and Centre for Sustainable Chemical Technologies, University of Bath, Claverton Down, Bath, BA2 7AY, United Kingdom.

*Corresponding author at:

Department of Chemical Engineering and Centre for Sustainable Chemical Technologies, University of Bath, Claverton Down, Bath, BA2 7AY, United Kingdom.

Tel: 0044 1225 385312, Fax: 0044 1225 385713, Email: eaep20@bath.ac.uk

Abstract

The spinning cloth disc reactor (SCDR) is an innovative enzymatic reaction intensification technology. The SCDR uses centrifugal forces to allow the spread of thin film across the spinning disc which has a cloth with immobilized enzyme. Research has shown this geometry promotes accelerated reactions due to high mass transfer rates and rapid mixing. In this study, the flow regimes in the SCDR were characterized by means of residence time distribution (RTD) analysis and visual study tracking dye staining.

RTD analysis showed that the flow pattern on the spinning disc with/without cloth became closer to plug flow with an increase of spinning speed and flow rate. With the cloth, the equivalent number of tanks-in-series was at least 2 times lower than that without cloth at different spinning speeds and flow rates, indicating the flow is better mixed, in contrast to the typical plug flow found for conventional spinning disc reactor. Two flow regimes were observed in the visual study with the dye spreading within the spinning cloth: radial finger-like flow and concentric flow. At low spinning speeds and high flow rates, the flow was in the form of a few random and uneven radial streams, with the zone between these streams free of dye. At higher spinning speeds and lower flow rates, this uneven radial flow was replaced by an even concentric flow. Using tributyrin hydrolysis as a model reaction, a SCDR reactor mathematical model based on perfectly mixed model was developed to simulate the variation in SCDR conversion with spinning speed and flow rate, and the model fitted well with the experimental data. The overall results indicate the SCDR is neither a conventional spinning disc reactor nor a rotating packed bed, but a separate class of spinning disc-type reactor for process intensification. This new reactor class is called ‘spinning mesh disc reactors’ (SMDRs), enabling any type of mesh (not just cloths) with an unbound top surface on a spinning disc to be included.

Keywords: spinning cloth disc reactor; lipase immobilization; residence time distribution; visualization; flow characteristics; mathematical modeling.

1. Introduction

Process intensification is considered as a promising development path for the chemical process industry, aiming to improve production efficiency, lower cost, enhance safety and reduce environmental pollution [1]. The spinning disc reactor (SDR) is one such process intensification technology, which consists of a rotating disc with a jet of liquid impinging onto the center of top surface of the disc. The centrifugal force of the spinning disc forces this liquid to form a thin and highly sheared film on top of the rotating surface, leading to rapid mixing and short residence times. Research has shown that the heat and mass transfer in such devices can be significantly enhanced by the fluid dynamics within these films [2-4]. The SDR has been applied in a wide range of chemical reactions such as polymerization [5], nanoparticle preparation [6-9], photocatalysis [10, 11], and transesterification in biodiesel synthesis [12]. The rotating packed bed (RPB) reactor, as a novel multi-phase contactor, is another reactor type which also uses centrifugal acceleration as driving forces to intensify mass transfer rate [13, 14]. In the RPB, the liquid sprays on the inside of the packed bed and spreads outwards by the centrifugal force. The gas is introduced from the outside and flows inward (counter-currently) to the liquid. The RPB has been reported to use in distillation [15], nanofibers and nanospheres preparation [16, 17], photocatalysts preparation [18], adsorption [19-21] and catalytic reactions [22].

Recently, the SDR concept has for the first time been introduced to immobilized enzymatic reactions as a novel rotating reactor system: the spinning cloth disc reactor (SCDR). Previous work has proven the feasibility of the SCDR in tributyrin emulsion hydrolysis, and its high efficiency in terms of reaction rates, conversion and stability was highlighted in comparison

to the conventional batch stirred tank reactor (BSTR) [23]. Based on the principles of the SDR, the SCDR also uses centrifugal forces to allow the spread of a thin film across a spinning horizontal disc; however this disc has a cloth (with thickness of 1.5 mm) with immobilized enzyme resting on top of it. The SCDR therefore produces a flow of thin film both on top of, as well as through the cloth, thus providing more effective surfaces for reaction. The cloth is critical to increasing the potential of immobilized enzymes in a variety of reactions, since it should produce accelerated reaction rates due to high mass transfer rates and rapid mixing on top of and within the cloth, with the cloth potentially helping protect the attached enzymes from excessive hydrodynamic forces, as well as providing an additional structure that can promote mixing and turbulence at the appropriate spinning speeds and flow rates. Therefore, the SCDR has characteristics of both the SDR and RPB: the cloth spins on the disc and is fed liquid like an SDR, but the liquid flow is interrupted by the cloth mesh, giving the flow on the disc characteristics that may be more like that in a RPB. Consequently both systems will be used in the analysis of the SCDR in this work.

The most popular techniques adopted in characterizing the flow regimes in the SDR and the RPB are visual quantification studies (through taking images with a conventional camera or a high speed camera) and residence time distribution (RTD) techniques.

For the SDR, it has been reported that several flow regimes can form on the spinning disc: smooth waves, concentric waves, spiral, irregular waves and film break up, which change with the spinning speeds, flow rates and physical property of liquid [24, 25]. Boiarkina *et al*. [4, 10] observed the boundaries of different water waves with a high speed camera at spinning speeds of 50- 400 rpm and flow rates of 5-35 mL s^{-1}. Mohammadi *et al*. [26] found that the RTD in SDR became narrower as the increase of spinning speeds and flow rates, implying the flow behavior became closer to ideal plug flow.

For the RPB, liquid is usually assumed to flow as thin films on the packing surface for the simplicity of modeling purpose. However, visual observations have indicated that liquid is travelling through the packing in uneven rivulets and droplets rather than film flow, which causes a maldistribution of liquid and hence decreases the overall efficiency of the reactor [27, 28].

The flow properties on a spinning disc have been studied with both RTD and visual techniques [10, 26], however, the introduction of the cloth will affect the flow properties, and the reported results of flow regimes in the SDR therefore may not be applicable to the SCDR. Consequently, the flow regimes in the SCDR need to be characterized to get a more in-depth understanding of flow characteristics and patterns to allow for better process control as well as reactor modeling and design. As such, the aim of this research is to characterize the flow regimes in the SCDR by means of RTD analysis and visual studies with dye, for a range of spinning speeds and flow rates. These results will be compared to the SDR and the RPB, and used to further model the reaction rate and conversion in the SCDR with respect to spinning speeds and flow rates using tributyrin hydrolysis as a model reaction and immobilized lipase on woolen cloth as the biocatalyst.

2. Materials and methods

2.1. Materials

Unbleached organic woolen cloth (color: natural cream, thickness: 1.5 mm) was purchased from Treliske (Otago, New Zealand). Amano lipase derived from *Pseudomonas fluorescens*, polyethyleneimine (PEI), tributyrin (98 %), tritonX-100, coomassie brilliant blue G 250, sodium bicarbonate and sodium carbonate were obtained from Sigma-Aldrich (New Zealand). Glutaraldehyde (GA) 25 % (w/v), sodium dihydrogen phosphate, disodium hydrogen phosphate, hydrochloric acid and potassium chloride were purchased from Unilab (ECP, New

Zealand). Hydrogen peroxide 30 % (v/v) was obtained from Scharlau (Thermofisher, New Zealand). Bovine serum albumin was obtained from Gibcobrl (Life Technologies, New Zealand). The water color dyes (Reeves, UK) were obtained from a local market. All solutions were prepared using deionized water (produced from Milli-Q Gradient A10 made by Millipore).

2.2. Preparation of immobilized lipase on woolen cloth

The main immobilization procedure has been described in detail by Feng *et al*. [29]. The woolen cloth was cut into circular pieces with a diameter of 250 mm, weighing 16 g. First, the woolen cloth was pretreated with a solution of 30 mL L^{-1} hydrogen peroxide (30 %) and 2 g L^{-1} sodium silicate at pH 9 (0.1 M Na_2CO_3, $NaHCO_3$ buffer) at 55 °C for 70 min. The bleached woolen cloth was then dipped in 500 mL 2 % PEI solution at pH 8 (adjusted with hydrochloric acid) for 2 h at room temperature and rinsed with deionized water. The cloth was thereafter soaked in 1 L 2 mg mL^{-1} lipase solution (0.1 M phosphate buffer, pH 6) for 24 h, followed by immersion in 500 mL 0.5 % (w/v) GA solution (0.1 M Na_2HPO_4, NaH_2PO_4 buffer, pH 6) for 10 min to achieve crosslinking. The cloth was finally washed with deionized water until no free enzyme was detected in the washed solution. The enzyme loading was 46.8 mg per dry gram of cloth determined by measuring the protein content of the enzyme solution with the Bradford method before and after immobilization [30]. The enzyme activity was 178.3 U per dry gram of woolen cloth determined by using the tributyrin emulsion hydrolysis method previously described by the authors [29].

2.3. Equipment

The SCDR mainly consists of a liquid feeding system, an overhead stirrer connected to a disc, a vessel for catching, containing and funneling liquid from the disc, and a reactant solution storage vessel, as shown in Fig. 1a. The cloth supporting spinning surface in this SCDR was a

Perspex disc with 250 mm in diameter, driven by a variable speed motor (Glas-Gol, US). The woolen cloth with immobilized lipase was rested (with no means of fastening) on the disc as shown in Fig. 1b. This spinning disc was enclosed in a steel funnel-shaped chamber 300 mm in diameter and 210 mm deep, which collected the liquid as it spun off the disc and channeled it to the storage vessel. Further details can be found in our previous publication [23].

The tributyrin emulsion was prepared by adding tributyrin and triton X-100 to the desired volume of phosphate buffer (0.1 M, pH 7) with a final concentration of 10 g L^{-1} and 3.5 g L^{-1}, respectively. The mixture was then emulsified with a motor homogenizer (IKA T25 digital, Japan) at 12,000 rpm for 5 min. The reaction was performed at 45 °C for 4 h. During the hydrolysis, sodium hydroxide was added into the reactant vessel with a pH stat to keep a constant pH and the data was collected continuously with a PC via the Tiamo 1.3 program (Metrohm, Switzerland). Reaction conversion was correlated to moles of sodium hydroxide consumed by the reaction according to Eq. 1:

$$Conversion(\%) = \frac{moles\ of\ free\ butyric\ acids}{moles\ of\ original\ esters\ in\ tributyrin} \times 100 \quad (1)$$

2.4 RTD study

A schematic diagram of the equipment set-up for the RTD study is shown in Fig. 1a. The cloths with immobilized lipase prepared as described in Section 2.2 were used for RTD study. The experiment was carried out at 20 °C. A solution of 0.5 M KCl was used as a tracer and deionized water was used as a test fluid. The tracer conductivity and concentration showed a good linear relationship for a concentration range between 0.005 and 0.5 M. The RTD could therefore be directly related to the conductivity of the tracer. A conductivity probe (Mettler Toledo, Switzerland) was placed in a small vessel (height of 37 mm, volume of 17 mL, and liquid holdup volume of 13.5 mL with conductivity probe in it) which collected the outlet

solution continuously and the data was logged to a PC every second with LabX direct software (Mettler Toledo, Switzerland).

Firstly, the deionized water was fed to the reactor at the desired spinning speed and flow rate until the reading of the conductivity meter in the outlet was stabilized and close to that of deionized water. Then, 1 mL of KCl was injected quickly to the center of the spinning disc with a syringe. The change in concentration in the outlet was measured as a function of time.

The analysis method used has been taken from literature [26, 31]. For the pulse injection of the tracer, the distribution density function of the residence time $E(t)$ can be calculated from Eq. 2 and it describes in a quantitative manner how much time different fluid elements have spent in the reactor.

$$E(t) = \frac{c(t)}{\int_0^t c(t)dt} = \frac{c(t_i)}{\sum_0^{t_{max}} c(t_i)\Delta t_i} \tag{2}$$

The mean residence time can be obtained as follows:

$$\bar{t} = \frac{\int_0^\infty tE(t)dt}{\int_0^\infty E(t)dt} = \int_0^\infty tE(t)dt = \frac{\sum_0^{t_{max}} t_i c(t_i)\Delta t_i}{\sum_0^{t_{max}} c(t_i)\Delta t_i} \tag{3}$$

The variance of RTD, σ_t^2, stands for the discrete level. A lower σ_t^2 means a narrow distribution and it can be obtained from Eq. 4:

$$\sigma_t^2 = \frac{\int_0^\infty \left(t-\bar{t}\right)^2 E(t)dt}{\int_0^\infty E(t)dt} = \int_0^\infty t^2 E(t)dt - \bar{t}^2 = \frac{\sum_0^{t_{max}} t_i^2 c(t_i)\Delta t_i}{\sum_0^{t_{max}} c(t_i)\Delta t_i} - \bar{t}^2 \tag{4}$$

The dimensionless forms of t, σ_t^2, $E(t)$ can obtained from Eq. 5 to 7

$$\theta = \frac{t}{\bar{t}} \tag{5}$$

(6)

$$\sigma_\theta^{\,2} = \frac{\sigma_t^{\,2}}{\bar{t}^{\,2}}$$

$$E(\theta) = \bar{t}E(t) \tag{7}$$

The number of tanks-in-series (N) is widely used to indicate if a flow is close to plug flow or not. The dimensionless distribution density function $E(\theta)$ can be obtained as follows:

$$E(\theta) = \frac{N^N}{(N-1)!}\theta^{N-1}e^{-N\theta} \tag{8}$$

N can be calculated as follows:

$$N = \frac{1}{\sigma_\theta^2} \tag{9}$$

As can be seen from Eq. 9, N is reversely related to the dimensionless form of the variance σ_θ^2, so N should be as be as high as possible to give an ideal plug flow (N>50 is usually considered as small deviation from plug flow) [26, 31].

2.5 Visual study

A combination of dye and conductivity RTD analysis was employed to investigate the flow characteristics on/within the spinning cloth with immobilized enzymes. The equipment setup is the same as that for RTD analysis (Fig. 1a), just the feed was changed from deionized water to dye solution. The cloths with immobilized lipase prepared as described in Section 2.2 were used for visual study. The conductivity measurement was carried out as described in Section 2.4. A green water color was selected as the tracer due to its good solubility in water. The dye solution was made by dissolving the water color in 0.25 M KCl solution. For each run, deionized water was fed to the spinning cloth at the desired spinning speed and flow rate until the cloth was saturated and the conductivity reading was stable. The feed was then

switched to the dye solution. As soon as the dye came out at the center of the cloth, imaging was launched, and images were taken every second until the cloth was completely covered with the dye. In the meantime, the corresponding conductivity data was continuously recorded as in Section 2.4.

2.6 Reactor modeling in tributyrin hydrolysis

Tributyrin emulsion hydrolysis in the SCDR was chosen as a model reaction to establish the mathematical equation of reaction conversion in the SCDR at various spinning speeds and flow rates. The experimental data of tributyrin hydrolysis in the SCDR can be found in the previous study [23]. Results in this study will show that there are several different flow regimes in the SCDR, which change with spinning speed and flow rate. In addition, as will be shown in the RTD analysis, under most cases the flow in the SCDR is far from plug flow (N<50). Therefore, the conventional plug flow modeling used in SDR analysis could not be used (i.e. the integral of reaction in small pieces of circles over the entire cloth). However, as the liquid volume on the disc is very small in comparison to the total reactant volume and good mixing in the reactant tank is achieved (as shown by the RTD analysis), well mixed reactor (and perfect mixing) is a good approximation for the reactor model [32]. Therefore the mass balance for the entire system is given in eq. 10:

$$\frac{dC}{dt} = -\frac{V_r}{V_t} r' \tag{10}$$

Where V_r is the liquid volume in the reactor (m^3), V_t is the total liquid volume in the system (m^3), r' is the global reaction rate and C is the substrate concentration.

The flow on a spinning disc is usually assumed to be a series of fully developed laminar films, and this theory is widely used in modeling both the SDR and the RPB [4, 13, 14, 33]. Considering the similarity between the SCDR and the RPB/SDR, the film flow theory was

hence used here to model the SCDR. The film thickness within the cloth can be calculated with the following equation [4, 13, 14, 33]:

$$h = \left(\frac{3Q\nu}{2\pi r^2 \omega^2} \right)^{1/3} \tag{11}$$

Where Q is the volumetric flow rate ($m^3\ s^{-1}$); υ is the kinematic viscosity ($m^2\ s^{-1}$); ω is the spinning speed (rad s^{-1}).

Therefore the liquid volume on the disc can be obtained by integration of the above equation:

$$V_r = \left(\frac{81Q\nu\pi^2}{16\omega^2} \right)^{1/3} R^{4/3} \tag{12}$$

It has been shown that, in the case of immobilized enzyme, the global reaction rate may be represented by a simple rate equation using apparent parameters and the interfacial concentration [34-36]. The mass balance of the substrate on the surface is then given by:

$$k_L a \left(C - C_i \right) = r' \tag{13}$$

Where k_La is the global mass transfer coefficient (s^{-1}), C is the substrate concentration in the bulk solution (mol m^{-3}), and C_i is the substrate concentration at the interface (mol m^{-3}).

The kinetics of tributyrin hydrolysis complies well with the Ping Pong Bi Bi mechanism [23, 37]:

$$r' = \frac{\left(v_{\max}{}' / K_m{}' \right) C_i}{1 + \left(C_0 - C_i \right) / K_i'} \tag{14}$$

It should be noted that the kinetic constants v_{max}', K_m' and K_i' are apparent lumped ping pong kinetic constants, and their expressions can be found in a previous publication [23]. C_0 is the

initial concentration of glyceride.

Combining Eq.13 and 14 gives

$$k_L a\left(C - C_i\right) = \frac{\left(v_{\max}{}' / K_m{}'\right) C_i}{1 + \left(C_0 - C_i\right) / K_i'} \tag{15}$$

Then C_i can be denoted as follows:

$$C_i = \frac{\left(K_i' + C_0 + C + \left(v_{\max}{}' / K_m{}'\right) K_i' / k_L a\right) - \sqrt{\left(K_i' + C_0 + C + \left(v_{\max}{}' / K_m{}'\right) K_i' / k_L a\right)^2 - 4C\left(K_i' + C_0\right)}}{2} \tag{16}$$

Combining Eq. 10, 12 and 16 gives

$$\frac{dC}{dt} = -\frac{\left(\frac{81 Q \nu \pi^2}{16 \omega^2}\right)^{1/3} R^{4/3}}{V_t} \frac{\left(v_{\max}{}' / K_m{}'\right)\left[\left(K_i' + C_0 + C + \left(v_{\max}{}' / K_m{}'\right) K_i' / k_L a\right) - \sqrt{\left(K_i' + C_0 + C + \left(v_{\max}{}' / K_m{}'\right) K_i' / k_L a\right)^2 - 4C\left(K_i' + C_0\right)}\right]}{2 + \left(2C_0 - \left(K_i' + C_0 + C + \left(v_{\max}{}' / K_m{}'\right) K_i' / k_L a\right) + \sqrt{\left(K_i' + C_0 + C + \left(v_{\max}{}' / K_m{}'\right) K_i' / k_L a\right)^2 - 4C\left(K_i' + C_0\right)}\right) / K_i'} \tag{17}$$

In order to get the substrate concentration at a given time from Eq. 17, the values of the parameters $k_L a$, v_{max}'/K_m' and K_i' were evaluated by using the inherent ode45 of MATLAB (MathWorks, Natick) from the previous experimental data at various spinning speeds and flow rates in the SCDR [23].

3. Results and discussion

3.1 RTD with pulse injection

To characterize the flow pattern on the spinning disc with/without cloth, RTD with pulse injection was investigated at various spinning speeds and flow rates. Fig. 2 shows the normalized RTD curve on the spinning disc with/without cloth. Generally, a very narrow RTD curve means that the flow pattern is close to ideal plug flow, and in contrast, a very broad RTD curve represents a large deviation from plug flow, where dispersion becomes more prominent [31]. As can be seen from Fig. 2, both with and without the cloth, with an increase of the spinning speed and flow rate, the RTD curve peaks became sharper and more narrow, which means that the flow pattern on the spinning disc with/without cloth becomes more close to ideal plug flow and thus the effect of dispersion on the radial flow direction is less significant. This is consistent with the results on the spinning disc observed by Mohammadi *et al*. [26], where they explained that a uniform velocity profile in the direction perpendicular to the flow direction and negligible dispersion in the direction of flow can be achieved at higher spinning speeds and flow rates, thus resulting in a near plug flow behavior. After placing the cloth on the disc, the RTD curve became more symmetric, especially at higher spinning speeds, indicating that a more even mixing on/within the cloth was achieved compared to that without cloth. Previous studies have reported that the waves on the spinning disc changed from smooth to spiral and unstructured with an increase of the spinning speed [10, 24], so an unstructured wave might be a reason for the more asymmetric RTD curve for the disc without cloth. In addition, longer tails (representing a wider range of residence times) were observed in comparison to that without the cloth (the tail was more obvious at low spinning speeds and flow rates), for example, the tail in Fig. 2a (without cloth) ended as the normalized residence time θ increased to 2.5, but the tail in Fig. 2b (with cloth) still existed

even for θ= 3. The longer tails at lower spinning speeds observed for the disc with the cloth may indicate that insufficient centrifugal forces were present to overcome the hydrodynamic resistance presented by the cloth and its constituent fibers, producing a greater range of fluid pathways the fluid is forced to follow (such as along the fibers and through some of the pathways of least resistance). At higher spinning speeds, these resistances are overcome enabling the fluid to bypass these pathways and take a more direct route (narrowing the residence time distribution and removing the observed tails in the distribution). In addition, long tails have been found to be an indication of laminar flow or stagnation areas [38-40]. This may also indicate that the existence of cloth could alleviate the turbulence on the disc, making the laminar flow better developed. However, the tail decreased with an increase of the spinning speed and the flow rate, and the RTD curve became more symmetric with an increase of flow rate. The effect of the cloth on tails are similar to that from Mohammadi *et al.* [26], where tails were observed on a grooved spinning disc (in comparison to a smooth disc), however they attributed this to the accumulation of liquid in the grooves. They also observed a decrease of tail with an increase of spinning speed and flow rate.

Fig. 3 shows the mean residence time versus spinning speed of disc with and without cloth. It can be seen that after adding the cloth onto the disc, the mean residence time nearly doubled, which would allow more contact time between the immobilized enzyme and substrate on/within the cloth. In addition, as expected, the mean residence time decreased with the increase of spinning speed and flow rate in both cases. It should be noted that the residence time here is larger than that previously reported for any SDR, which is usually a few seconds [41]. This is because the residence time measured here includes not only the period from the inlet to the edge of the disc but also the extra period from the edge of the disc to the final outlet. However, this extra time was the same throughout all the experiments (estimated to be around 7 s). As the main purpose of this RTD study here was to characterize

the effect of spinning speed and flow rate on the flow pattern on the spinning cloth, the measuring error mentioned above was insignificant. To obtain more accurate residence time on the disc, the reactor would need to be redesigned to accommodate a conductivity probe at the edge of the disc, as well as a liquid holdup there to allow a conductivity probe to operate. As we did not want to redesign the reactor (as we are characterizing flow in a reactor which already has reaction data available [23], this was considered infeasible.

A large number of tanks-in-series (N) means that the flow pattern is close to plug flow (N>50 is usually considered as a small deviation from plug flow) [26, 31]. As can be seen from Fig. 4, N increased with an increase of spinning speed and flow rate, for example, as the spinning speed and flow rate increased from 50 rpm, 2 mL s^{-1} to 500 rpm, 8 mL s^{-1}, N increased from 2 to 10 for the disc with cloth and increased from 5 to 23 for the disc without cloth, indicating the flow was getting close to plug flow. This is consistent with the result from Fig 2. At a spinning speed of 50 rpm, due to smaller centrifugal forces, the mixing efficiency on the disc with/without cloth was low and the aforementioned hydrodynamic resistances created by the cloth are not sufficiently overcome, hence the residence time was longer. At this condition, the dispersion of the tracer became more pronounced, resulting in a larger deviation from the plug flow; therefore a smaller N (4 for the disc without cloth) was obtained even at the higher flow rate of 8 mL s^{-1}. It can be concluded that at such low spinning speeds, the spinning speed is more dominant in determining the flow pattern. In comparison, as the spinning speed increased to 150 rpm, N increased significantly (almost by twice). This behavior implied a significant improvement in mixing, since the centrifugal forces gained impact (e.g. overcoming the aforementioned hydrodynamic resistances). After this, the flow rate was a more critical factor in determining the flow pattern and the mixing. In addition, N for the disc without cloth was at least twice higher than that with cloth, again indicating that the cloth will cause more significant dispersion and hence larger deviation from plug flow, which is in

good agreement with the RTD curves in Fig. 2. Under similar spinning speeds and flow rates, the *N* found here was comparable to that from Mohammadi *et al*. [26], where it was estimated to be approximately 26-42 at a spinning speed of 300-1200 rpm and flow rate of 10 mL s^{-1}, indicating the RTD result here is not out of ordinary.

3.2 Flow characteristics with imaging analysis

The RTD analysis indicates that the SCDR had a larger deviation from plug flow compared to the SDR, and that the flow pattern of both reactors were getting close to plug flow with an increase of spinning speed and flow rate. However, very little information can be derived in terms of the flow characteristics that determine this RTD. Therefore, a visual observation of flow regimes in the SCDR was undertaken in combination with a RTD analysis. The results from the visual analysis will be presented first.

3.2.1 Bulk flow characteristics

As can be seen from Fig. 5, the momentum of the injected liquid allowed it to quickly penetrate through the whole cloth. Close to the injection area, the liquid was accelerated to the disc spinning speed by the interaction with the cloth. The tangential forces from spinning disc were able to generate a relatively uniform distribution of liquid, which can be observed at all investigated spinning speeds and flow rates. However, beyond this initial fluid speed up area at the disc center, two different flow regimes were observed within the cloth which vary with disc spinning speed and flow rate. At a low spinning speed of 100 rpm (Fig. 5a-d), the dye spread unevenly, transporting across the cloth via a small number of radial streams, with the liquid front in each moving at different speeds (dictated by the hydrodynamic resistance encountered and volume of liquid in the particular radial stream). The shapes of these radial streams look like fingers, so they are named “radial finger-like streams” throughout the manuscript to be more easily understood. With an increase of flow rate (Fig. 5a-d), more

radial finger-like streams were formed. When the spinning speed increased to 250 rpm (Fig. 5e-h), the spreading patterns changed with the flow rate. For example, for the flow rate of 2 mL s^{-1} (Fig. 5e) the dye spread concentrically and evenly, but when the flow rate increased to 3.5 mL s^{-1} (Fig. 5f), a transition state was observed: a combination of concentric and radial finger-like spreading. When flow rate further increased to 5 mL s^{-1} (Fig. 5g) and above (Fig. 5h), the spreading completely changed back to radial finger-like streams. For the highest spinning speed of 400 rpm, the transition state changed from flow rate of 3.5 mL s^{-1} to 5 mL s^{-1}. For the flow rate of 3.5 mL s^{-1} (Fig. 5j), it had completely transferred from the transition state to concentric flow. For the flow rate of 5 mL s^{-1} (Fig. 5k), the flow type was a combination of concentric and radial flow (transition state), and more radial finger-like streams can be observed compared to that at the lower spinning speed of 250 rpm (Fig. 5k and Fig. 5f). Images showing the development of different flow types over time are also provided in the Supplementary Material.

Therefore, for bulk flow, two different flow regimes types in the spinning cloth can be summarized: (1) radial finger-like flow and (2) concentric flow. For type 1 flow, the liquid flows with a few random and uneven radial finger-like streams on the spinning cloth, with the zones between streams free of dye. In addition, the numbers of the streams can be adjusted by the feed flow rate: the higher the flow rate, the more streams on the cloth. For type 2, the liquid flows with even concentric streams on the spinning cloth.

The distribution of flow regimes with different spinning speeds and flow rates are shown in Fig. 6. The spinning speed determines the flow regime at lower spinning speeds (100 rpm), and type 1 flow (radial finger-like flow) was observed at all flow rates. With an increase of spinning speed, the flow rate becomes the dominant factor determining if the flow regime in the spinning cloth was type 1 or 2: the flow rates below 5 mL s^{-1} produced type 2 flow (concentric flow), and the flow rates tested above this switched the flow back to type 1 (at the

spinning speeds tested above 100 rpm). In addition, the transition state between type 1 and type 2 could also be observed at 250 rpm and 3.5 mL s^{-1}, 400 rpm and 5 mL s^{-1}.

The results found here are also comparable to those observed previously by Burns *et al*. [27, 28] in the RPB, indicating that the SCDR has some flow characteristics similar to this technology. They found that the main flow was in the form of radial rivulets at low rotational speeds between 300-600 rpm with flow rate of 10.5 L min^{-1}. With an increase in rotational speed, the level of maldistribution via these radial rivulets was decreased. This is similar to the results here, where radial streams were observed with spinning speed below 100 rpm, and transferred to concentric flow as with the increase of spinning speed with a clear transition state.

The two different flow types can be explained by considering the two dimensional flow on/within the cloth, which was first proposed for spinning disc by Wood and Watts [42]. The two-dimensional flow which incorporates inertial and viscous influences existed over a spinning disc. In SCDR, the main forces working on the fluid are centrifugal force, viscous force and inertia force. The centrifugal force is always the driving force. The viscous force (drag by the viscosity of fluid) and inertial force (caused by the natural liquid flow paths changes within the cloth) are resistances and influenced by spinning speeds and flow rates, so they may take turn to dominate the resistance under different conditions [43, 44]. At low spinning speed and high flow rate, the main resistance is from the viscous drag force, and the inertial force is unimportant (dissipation by the flow paths changes within cloth), so the liquid within the cloth is not likely to change flow paths frequently and presents a few radial finger-like streams, which was observed as type 1 flow. At high spinning speed and low flow rate, the main resistance is from the inertial force, and the viscous force is unimportant. Therefore most energy is consumed by the liquid flow paths changes within the cloth, the tangential flow prevails more than the radial flow, resulting in the type 2 flow. However, at medium

spinning speeds and flow rates, both viscous forces and inertia forces are significant and result in the coexistence of radial flow and tangential flow, which was observed as the transition area.

3.2.2 Surface flow - droplets on cloth

Besides the bulk flow described above, under all investigated range of spinning speeds and flow rates, a small part of the liquid also existed in the form of droplets on the surface of the spinning cloth, which moved in a spiral pattern, as shown in Fig. 7 (the white points on the cloth). This type of surface flow is more similar to a conventional SDR than a RPB. The volume of the droplets observed is much lower than the liquid volume being fed to the reactor indicating that this is not a major flow path under the spinning speeds and flow rates studied. In addition, the number of droplets was found to increase with decreasing of spinning speed and increasing of flow rate, which may be due to the higher liquid holdup in the cloth at low spinning speeds and high flow rates.

3.2.3 Correlating RTD with the visual analysis

By comparison of RTD to imaging analysis at the different spinning speeds and flow rates, it appears (unexpectedly) that there is no significant correlation between flow type and RTD. This is exemplified by the fact that in the RTD analysis, *N* increased and the flow was close to plug flow for both radial flow and concentric flow with increases of the spinning speeds and flow rates. RTD is mainly determined by the mixing of fluid in the cloth, so the fact that the flow type difference does not significantly correlate to changes in the RTD may indicate the two flow types can achieve a similar extent of mixing within the cloth.

To confirm this, in conjunction with the dye study, the corresponding conductivity was also measured at the outlet to compliment the dye result, as shown in Fig. 8. In these experiments,

the conductivity in the outlet increased until it eventually stabilized. The increasing region can be related to the period of dye spreading across and through the cloth. With an increase of flow rate, the slope of the increasing region increased, indicating that the flow pattern is closer to plug flow. In theory, at the same flow rate, the residence time of the tracer should be shorter at higher spinning speed. However, as can be seen from Fig. 8a and Fig. 8d, the tracer concentration at the lowest spinning speed (100 rpm) at the outlet was higher than that of high spinning speed (250 and 400 rpm), and this can be attributed to the uneven radial flow on the spinning cloth: even at low spinning speed, some tracer may reach the edge of the cloth very fast in the form of the radial flow. This is in good agreement with the image results and indicates that RTD studies are affected by mixing and other phenomena that is not necessarily reflected by the bulk fluid movement in the cloth (as seen in the visual analysis).

3.3 Implications to reaction conversion, reactor/kinetic modeling and reactor classification of the SCDR

3.3.1 Flow regime vs. Reaction conversion

The correlation between spinning speed and flow rate with tributyrin hydrolysis conversion and flow regime in the SCDR within 1 h is shown in Fig. 6. The conversion increased with an increase of spinning speed and flow rate within the investigated range. It should be noted that a distinct increase in conversion was observed when the spinning speed increased from 250 rpm to 400 rpm and the flow rate increased from 2 mL s^{-1} to 5 mL s^{-1}. This might be related to the transition of flow regimes from concentric flow to radial flow. Other than this, the flow regimes do not appear to have a significant relationship to changes in the reaction conversion. This is similar with a previous study, where the wave regimes on the spinning disc were found to have no influence on the reaction kinetics [10]. Note that the highest reaction conversion was obtained in type 1 (radial finger-like) flow at the higher spinning speeds and

higher flow rates. A higher conversion would necessitate that a greater cloth volume to be wetted by the reactant and a greater amount of contact (with lower mass transfer resistance) between the reactant and the active enzymes as well as a higher volume of liquid processed per pass (as expected at the higher flow rates) to allow more tributyrin to converted. Since this flow region is beyond the concentric flow where it is clear that the entire cloth is being wetted, this result may also indicate that the radial finger-like flow at the higher flow rates is characteristic of a fully wetted cloth (as per concentric flow) where the higher fluid flow rate and higher spinning speed (and therefore centrifugal force) allows more fluid through the paths of least resistance in the cloth (as they did at the lower spinning speeds and flow rates). Therefore more fluid is able to contact the enzymes at the decreased mass transfer resistances produced at the higher flow rates and spinning speeds combined with a higher fluid volume per pass in the reactor, producing the higher conversion.

3.3.2 Reactor model and kinetic modeling

The RTD and visual analysis of the SCDR above indicates that the flow is far from plug flow under a majority of the investigated conditions, meaning that the entire SCDR system overall meets the requirements of a well-mixed reactor (under the perfect mixing model), validating the model of this system proposed in Eq. 10 to Eq. 17. So, from this, the apparent kinetic constants v_{max}'/K_m' and K_i' could be and were estimated to be 0.494 s^{-1} and 1.088 mol m^{-3} respectively. The estimated global mass transfer coefficients k_La from Eq. 17 at various flow rates and spinning speeds were shown in Table 1. It is observed that k_La increased from 0.614 to 1.331 s^{-1}, and 0.769 to 1.462 s^{-1} as the spinning speed increased from 250 to 500 rpm for the flow rates of 2 mL s^{-1} and 5 mL s^{-1} respectively. This increasing trend in the SCDR is similar to that reported in the SDR [45] and the RPB [13], which may be due to the intensified turbulence at higher spinning speeds and flow rates.

An example of the time course of tributyrin hydrolysis from experiment and modeling at selected spinning speeds and flow rates is shown in Fig. 9, showing a good match between the model and the experimental data for individual reaction conditions. Looking at the reaction data as a whole, Fig. 10 shows the validation of the proposed model by comparing the conversion predicted from the model at different spinning speeds and flow rates to that from the experimental data. The reaction features in Fig. 10 has already been explained in our previous paper [23]. Fig. 10 shows that the SCDR reactor model gives reasonably good agreement with the experimental data, especially at the lower flow rate (2 mL s^{-1}) where the reactor is closer to being a well-mixed reactor. Overall, the model slightly overestimated the conversion for all the flow rates (<5 %), which might be attributed to the detachment/deactivation of enzyme caused by the high shear forces, which was not considered in this modeling. At the higher flow rate (5 mL s^{-1}), where the SCDR becomes closer to plug flow in its flow characteristics (RTD), the deviation between the model and the experimental data increased (as is also expected).

3.3.3 Implication to reactor classification

Overall, the combination of RTD results, visual analysis and well-mixed reactor modeling indicate that the SCDR is neither a conventional SDR (in particular due to it being well mixed) nor a RPB (in particular the surface flow) – it is a reactor with characteristics that are in-between these two. It is therefore a separate and new type of spinning disc-type reactor for process intensification, which therefore requires a classification. Due to the mixture of SDR and RPB characteristics, we propose that this new reactor class is known as ‘spinning mesh disc reactors’ which can be abbreviated as ‘SMDR’.

4. Conclusions

In this study, the flow regimes in the SCDR were characterized by RTD and visual study, and a model of the SCDR was proposed with respect to spinning speeds and flow rates using tributyrin hydrolysis as a model reaction and immobilized lipase on woolen cloth as the biocatalyst.

RTD analysis showed that the flow pattern on the spinning disc with/without cloth became close to plug flow with the increase of spinning speed and flow rate. The disc with cloth showed a larger deviation from plug flow pattern in comparison to that without the cloth, with the number of tanks-in-series (N) required to model the RTD two times smaller than that of the disc with cloth.

Two flow regimes were observed from the visual dye study: radial finger-like flow and concentric flow. At low spinning speed and high flow rate, the flow was in the form of a few random and uneven radial streams, with the zone between the streams free of dye. At higher spinning speeds and lower flow rates, the unevenly radial flow was replaced by an even concentric flow. There were also two regions of flow – within the cloth and on top of the cloth, showing that the SCDR acts both as a conventional SDR (with unbound flow on top of the cloth disc) and also partially like a RPB (with bounded flow within the cloth).

When comparing RTD, the visual study and previously determined reaction conversions however, no significant correlation between the different flow regimes and the RTD and the reaction conversion was found.

Based on the RTD and visual analysis, the SCDR reactor mathematical model based on perfectly mixed model was developed to simulate the variation in SCDR conversion with spinning speed and flow rate. The model fitted well with the experimental data, further

substantiating that the SCDR is a well-mixed reactor. The combination of RTD results, visual analysis and well-mixed reactor modeling indicate that the SCDR is neither a conventional SDR nor a RPB. It is therefore a separate and new type of spinning disc-type reactor for process intensification – a reactor class we call ‘spinning mesh disc reactors’, allowing any type of mesh (not just cloths) on a rotating disc with the top surface left unbound to be included.

Acknowledgements

The authors thank the China Scholarship Council for the PhD scholarship. The authors also thank Irina Boiarkina for helpful discussions. The authors also acknowledge Raymond Hoffmann, Peter Buchanan, Laura Liang, Allan Clendinning, Frank Wu, Jessie Matthew and Cecilia Lourdes, for their help in this work.

Nomenclature

C	substrate concentration in the bulk solution (mol m^{-3})
V_r	liquid volume in the reactor (m^3)
V_t	total liquid volume in the system (m^3)
r′	global reaction rate (mol m^{-3} s^{-1})
Q	volumetric flow rate (m^3/s)
υ	kinematic viscosity (m^2/s)
ω	spinning speed (rad/s)
h	film thickness (m)
r	distance between any point on the disc to the center (m)
R	constant, the radius of the disc (0.125 m)
C_i	substrate concentration at the interface (mol m^{-3})
C_0	initial concentration of the glyceride (mol m^{-3})
k_L	mass transfer coefficient (m s^{-1})
a	effective interfacial area per unit volume (m^{-1})
k_La	global mass transfer coefficient (s^{-1})
v_{max}'	apparent maximum reaction rate (mol m^{-3} s^{-1})
K_m'	apparent Michaelis-Menten constant for the glyceride (mol m^{-3})
K_i'	apparent inhibition constant for the fatty acid (mol m^{-3})

References

[1] T. Van Gerven, A. Stankiewicz, Structure, Energy, Synergy, Time-The Fundamentals of Process Intensification, Ind. Eng. Chem. Res., 48 (2009) 2465-2474.
[2] R.J.J. Jachuck, C. Ramshaw, Process intensification: Heat transfer characteristics of tailored rotating surfaces, Heat. Recov. Syst CHP., 14 (1994) 475-491.
[3] K.V.K. Boodhoo, R.J. Jachuck, Process intensification: spinning disc reactor for condensation polymerisation, Green Chem., 2 (2000) 235-244.
[4] I. Boiarkina, S. Norris, D.A. Patterson, Investigation into the effect of flow structure on the photocatalytic degradation of methylene blue and dehydroabietic acid in a spinning disc reactor, Chem. Eng. J., 222 (2013) 159-171.
[5] K.V.K. Boodhoo, R.J. Jachuck, Process intensification: spinning disk reactor for styrene polymerisation, Appl. Therm. Eng., 20 (2000) 1127-1146.
[6] C.Y. Tai, Y.H. Wang, H.S. Liu, A green process for preparing silver nanoparticles using spinning disk reactor, AIChE J., 54 (2008) 445-452.
[7] H.S. Liu, Y.H. Wang, C.C. Li, C.Y. Tai, Characterization of AgI nanoparticles synthesized in a spinning disk reactor, Chem. Eng. J., 183 (2012) 466-472.
[8] H.S. Liu, K.A. Chen, C.Y. Tai, Droplet stability and product quality in the Higee-assisted microemulsion process for preparing CaCO3 particles, Chem. Eng. J., 197 (2012) 101-109.
[9] B.C.Y. Chan, X. Wang, L.K.W. Lam, J.M. Gordon, D. Feuermann, C.L. Raston, H. Tong Chua, Light-driven high-temperature continuous-flow synthesis of TiO2 nano-anatase, Chem. Eng. J., 211–212 (2012) 195-199.
[10] I. Boiarkina, S. Pedron, D.A. Patterson, An experimental and modelling investigation of the effect of the flow regime on the photocatalytic degradation of methylene blue on a thin film coated ultraviolet irradiated spinning disc reactor, Appl. Catal. B-environ, 110 (2011) 14-24.
[11] I. Boiarkina, S. Norris, D.A. Patterson, The case for the photocatalytic spinning disc reactor as a process intensification technology: Comparison to an annular reactor for the degradation of methylene blue, Chem. Eng. J., 225 (2013) 752-765.
[12] Z. Qiu, J. Petera, L.R. Weatherley, Biodiesel synthesis in an intensified spinning disk reactor, Chem. Eng. J., 210 (2012) 597-609.
[13] S. Munjal, M.P. Dudukovic, P. Ramachandran, Mass-transfer in rotating packed beds. 1. development of gas-liquid and liquid-solid mass-transfer correlations, Chem. Eng. Sci., 44 (1989) 2245-2256.
[14] S. Munjal, M.P. Dudukovic, P. Ramachandran, Mass-transfer in rotating packed beds. 2. experimental results and comparison with theory and gravity flow, Chem. Eng. Sci., 44 (1989) 2257-2268.
[15] T. Kelleher, J.R. Fair, Distillation studies in a high-gravity contactor, Ind. Eng. Chem. Res., 35 (1996) 4646-4655.
[16] J.F. Chen, L. Shao, F. Guo, X.M. Wang, Synthesis of nano-fibers of aluminum hydroxide in novel rotating packed bed reactor, Chem. Eng. Sci., 58 (2003) 569-575.
[17] A.J. Nathanael, S.I. Hong, D. Mangalaraj, P.C. Chen, Large scale synthesis of hydroxyapatite nanospheres by high gravity method, Chem. Eng. J., 173 (2011) 846-854.
[18] C.C. Lin, Y.J. Chiang, Preparation of coupled ZnO/SnO2 photocatalysts using a rotating packed bed, Chem. Eng. J., 181 (2012) 196-205.
[19] Y.S. Chen, Y.C. Hsu, C.C. Lin, C.Y.D. Tai, H.S. Liu, Volatile organic compounds absorption in a cross-flow rotating packed bed, Environ. Sci. Technol., 42 (2008) 2631-2636.
[20] L.-J. Hsu, C.-C. Lin, Removal of methanol and 1-butanol from binary mixtures by absorption in rotating packed beds with blade packings, Chem. Eng. J., 168 (2011) 190-200.

[21] L.L. Zhang, J.X. Wang, Q. Sun, X.F. Zeng, J.F. Chen, Removal of nitric oxide in rotating packed bed by ferrous chelate solution, Chem. Eng. J., 181–182 (2012) 624-629.
[22] C.C. Chang, C.Y. Chiu, C.Y. Chang, C.F. Chang, Y.H. Chen, D.R. Ji, Y.H. Yu, P.C. Chiang, Combined photolysis and catalytic ozonation of dimethyl phthalate in a high-gravity rotating packed bed, J. Hazard. Mater., 161 (2009) 287-293.
[23] X. Feng, D.A. Patterson, M. Balaban, G. Fauconnier, E.A.C. Emanuelsson, The spinning cloth disc reactor for immobilized enzymes: A new process intensification technology for enzymatic reactions, Chem. Eng. J., 221 (2013) 407-417.
[24] A.F. Charwat, R.E. Kelly, C. Gazley, Flow and stability of thin liquid films on a rotating disk, J. Fluid Mech., 53 (1972) 227-255.
[25] H. Espig, R. Hoyle, Waves in a thin liquid layer on a rotating disk, J. Fluid Mech., 22 (1965) 671-677.
[26] S. Mohammadi, K.V.K. Boodhoo, Online conductivity measurement of residence time distribution of thin film flow in the spinning disc reactor, Chem. Eng. J., 207–208 (2012) 885-894.
[27] J.R. Burns, C. Ramshaw, Process intensification: Visual study of liquid maldistribution in rotating packed beds, Chem. Eng. Sci., 51 (1996) 1347-1352.
[28] J.R. Burns, J.N. Jamil, C. Ramshaw, Process intensification: operating characteristics of rotating packed beds - determination of liquid hold-up for a high-voidage structured packing, Chem. Eng. Sci., 55 (2000) 2401-2415.
[29] X. Feng, D.A. Patterson, M. Balaban, E.A.C. Emanuelsson, Enabling the utilization of wool as an enzyme support: Enhancing the activity and stability of lipase immobilized onto woolen cloth, Colloid Surf. B-Biointerfaces, 102 (2013) 526-533.
[30] M.M. Bradford, Rapid and sensitive method for quantitation of microgram quantities of protein utilizing principle of protein-dye binding, Anal. Biochem., 72 (1976) 248-254.
[31] O. Levenspiel, Chemical Reaction Engineering, 3rd ed., Wiley, New York, 1999.
[32] M.D. Ballari, O.M. Alfano, A.E. Cassano, Mass transfer limitations in slurry photocatalytic reactors: Experimental validation, Chem. Eng. Sci., 65 (2010) 4931-4942.
[33] J.R. Burns, C. Ramshaw, R.J. Jachuck, Measurement of liquid film thickness and the determination of spin-up radius on a rotating disc using an electrical resistance technique, Chem. Eng. Sci., 58 (2003) 2245-2253.
[34] R. Lortie, D. Thomas, Heterogeneous one-dimensional model for fixed-bed enzyme reactors, Biotechnol. Bioeng., 28 (1986) 1256-1260.
[35] R. Lortie, D. Pelletier, Comparison between dispersion and plug-flow models for fixed-bed enzyme reactors, AIChE J., 38 (1992) 1477-1480.
[36] C.R. Carrara, E.J. Mammarella, A.C. Rubiolo, Prediction of the fixed-bed reactor behaviour using dispersion and plug-flow models with different kinetics for immobilised enzyme, Chem. Eng. J., 92 (2003) 123-129.
[37] F.X. Malcata, C.G.H. Jr., C.H. Amundson, Hydrolysis of butteroil by immobilized lipase using a hollow-fiber reactor: Part II. Uniresponse kinetic studies, Biotechnol. Bioeng., 39 (1992) 984-1001.
[38] D. Boskovic, S. Lobbecke, A. Gross, M. Kohler, Residence Time Distribution Studies in Microfluidic Mixing Structures, Chem. Eng. Technol., 34 (2011) 361-370.
[39] J. Dubois, L. Tremblay, M. Lepage, P. Vermette, Flow Dynamics Within a Bioreactor for Tissue Engineering by Residence Time Distribution Analysis Combined With Fluorescence and Magnetic Resonance Imaging to Investigate Forced Permeability and Apparent Diffusion Coefficient in a Perfusion Cell Culture Chamber, Biotechnol. Bioeng., 108 (2011) 2488-2498.

[40] C. Gutierrez, E. Dias, J.A.W. Gut, Investigation of the residence time distribution in a plate heat exchanger with series and parallel arrangements using a non-ideal tracer detection technique, Appl. Therm. Eng., 31 (2011) 1725-1733.
[41] M. Vicevic, K.V.K. Boodhoo, K. Scott, Catalytic isomerisation of [alpha]-pinene oxide to campholenic aldehyde using silica-supported zinc triflate catalysts: II. Performance of immobilised catalysts in a continuous spinning disc reactor, Chem. Eng. J., 133 (2007) 43-57.
[42] R.M. Wood, B.E. Watts, Flow, heat and mass-transfer characteristics of liquid films on rotating disks, Trans. Inst. Chem. Eng., 51 (1973) 315-322.
[43] J.E. Buchanan, Holdup in Irrigated Ring-Packed Towers below the Loading Point, Ind. Eng. Chem. Fundam., 6 (1967) 400-407.
[44] A. Basic, M.P. Dudukovic, Liquid holdup in rotating packed beds: examination of the film flow assumption, AIChE J., 41 (1995) 301-316.
[45] F. Visscher, J. van der Schaaf, M.H.J.M. de Croon, J.C. Schouten, Liquid–liquid mass transfer in a rotor–stator spinning disc reactor, Chem. Eng. J., 185–186 (2012) 267-273.

Figure legends

Figure 1(a) Schematic diagram of the enzymatic reactor setup for the RTD and visual study of the SCDR. (b) Top view of a 25 cm diameter woolen cloth with immobilized lipase on the disc of the SCDR.

Figure 2 Effect of spinning speed on residence time distribution. (a) flow rate 2 mL s^{-1} without cloth; (b) flow rate 2 mL s^{-1} with cloth; (c) flow rate 5 mL s^{-1} without cloth; (d) flow rate 5 mL s^{-1} with cloth; (e) flow rate 8 mL s^{-1} without cloth; (f) flow rate 8 mL s^{-1} with cloth.

Figure 3 The mean residence time at different spinning speeds and flow rates. Results were from triplicate measurements and error bars are the average ± one standard deviation.

Figure 4 The number of tanks-in-series (*N*) at different spinning speeds and flow rates. Results were from triplicate measurements and error bars are the average ± one standard deviation.

Figure 5 Images of the dye spreading types on the spinning disc cloth with different spinning speeds and flow rates. All the images were at the same time of 12 s after injection of the dye.

Figure 6 The dependency of flow regimes and the reaction conversion on spinning speeds and flow rates in the SCDR.

Figure 7 Droplets on the spinning cloth at a spinning speed of 250 rpm and a flow rate of 5 mL s^{-1}.

Figure 8 The corresponding conductivity in the outlet versus time as the dye was continuously fed to the SCDR at various flow rates: (a) 2 mL s^{-1}, (b) 3.5 mL s^{-1}, (c) 5 mL s^{-1}, (d) 8 mL s^{-1}.

Figure 9 Time course of tributyrin hydrolysis in the SCDR. The scattered points are the continuous experimental data from the pH stat, while the solid lines are calculated from the

derived reactor model (Section 2.6): (a) flow rate: 2mL s^{-1}, spinning speed: 250 rpm; (b) flow rate: 5 mL s^{-1}, spinning speed: 500 rpm.

Figure 10 Conversion of tributyrin hydrolysis in the SCDR at various spinning speeds and flow rates. The scattered points are the experimental data, and the solid lines are from the derived reactor model (Section 2.6). Substrate concentration: 33 mM, feed volume: 1L, reaction time: 4 h. Half of the experimental data points were from triplicate measurements, and error bars are the average ± one standard deviation.

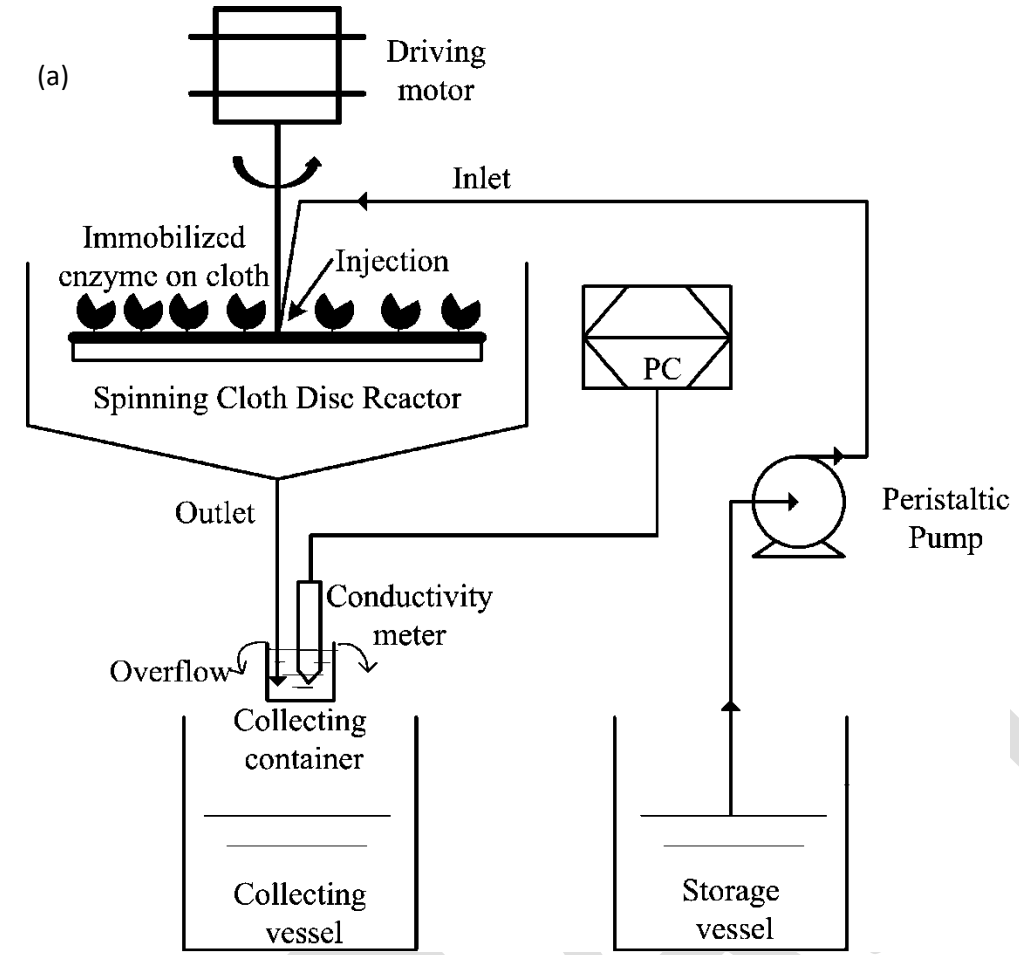
(a)
Driving motor
Inlet
Immobilized enzyme on cloth
Injection
PC
Spinning Cloth Disc Reactor
Outlet
Peristaltic Pump
Conductivity meter
Overflow
Collecting container
Collecting vessel
Storage vessel

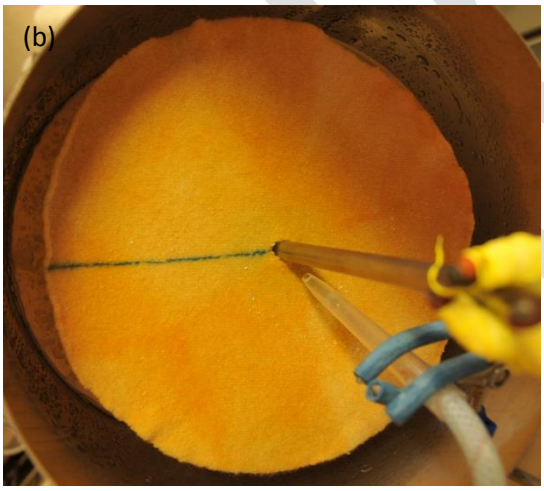
(b)

Figure 1

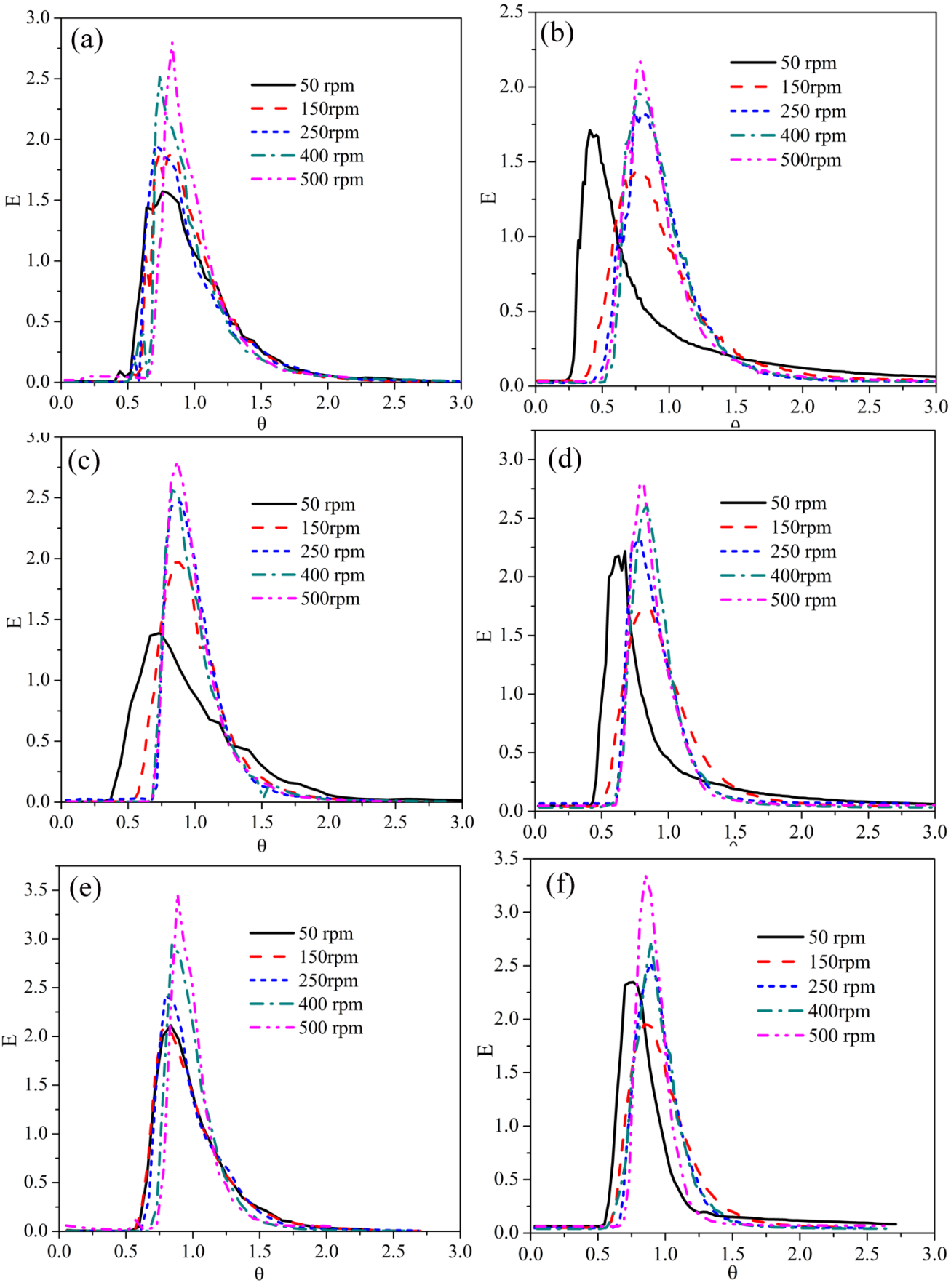
(a)
50 rpm
150rpm
250rpm
400 rpm
500 rpm
E
θ
(b)
50 rpm
150rpm
250 rpm
400 rpm
500rpm
E
θ
(c)
50 rpm
150rpm
250 rpm
400 rpm
500rpm
E
θ
(d)
50 rpm
150rpm
250 rpm
400rpm
500 rpm
E
θ
(e)
50 rpm
150rpm
250rpm
400 rpm
500 rpm
E
θ
(f)
50 rpm
150rpm
250 rpm
400rpm
500 rpm
E
θ

Figure 2

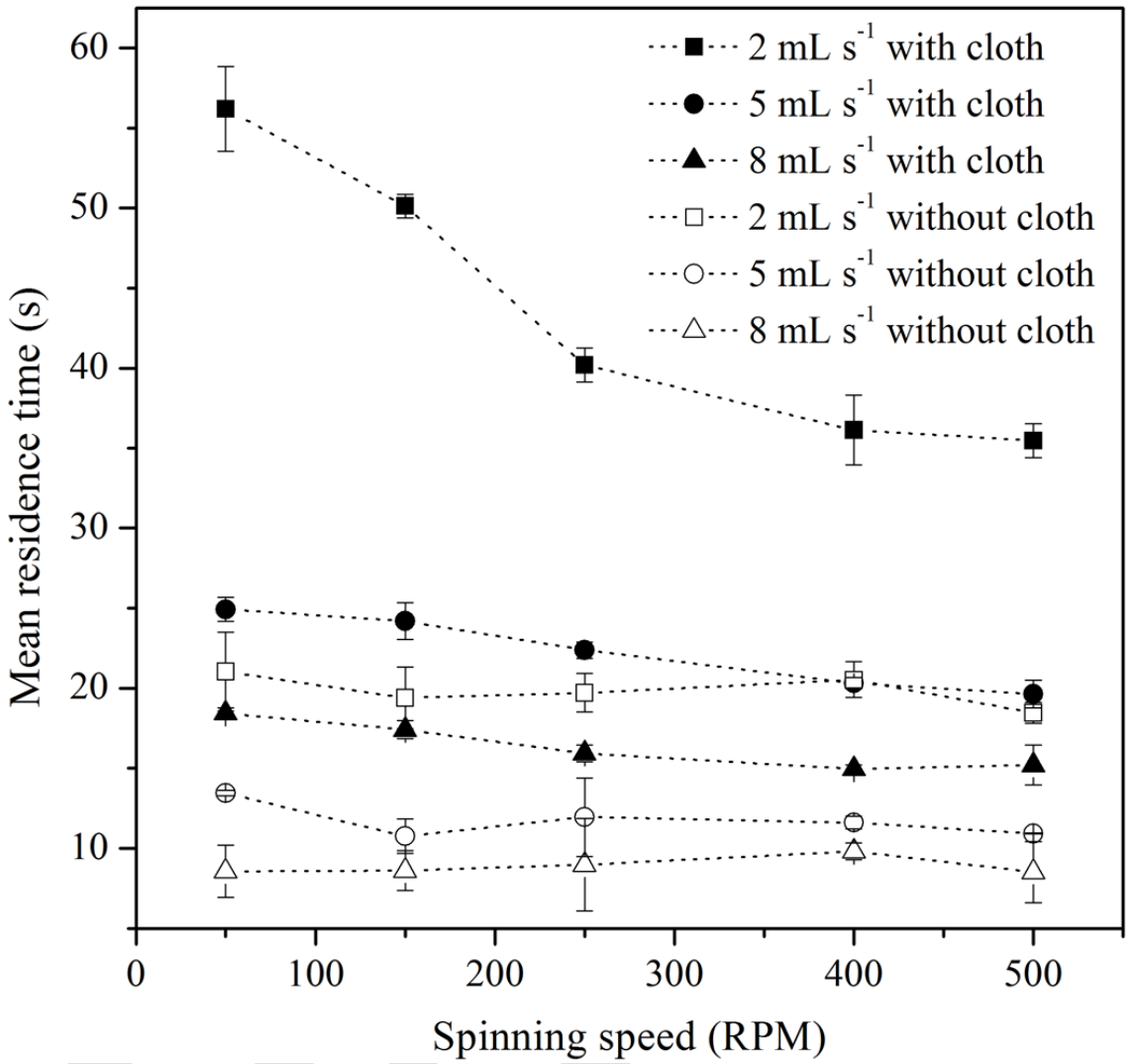
Mean residence time (s)
Spinning speed (RPM)
2 mL s-1 with cloth
5 mL s-1 with cloth
8 mL s-1 with cloth
2 mL s-1 without cloth
5 mL s-1 without cloth
8 mL s-1 without cloth
60
50
40
30
20
10
0
100
200
300
400
500

Figure 3

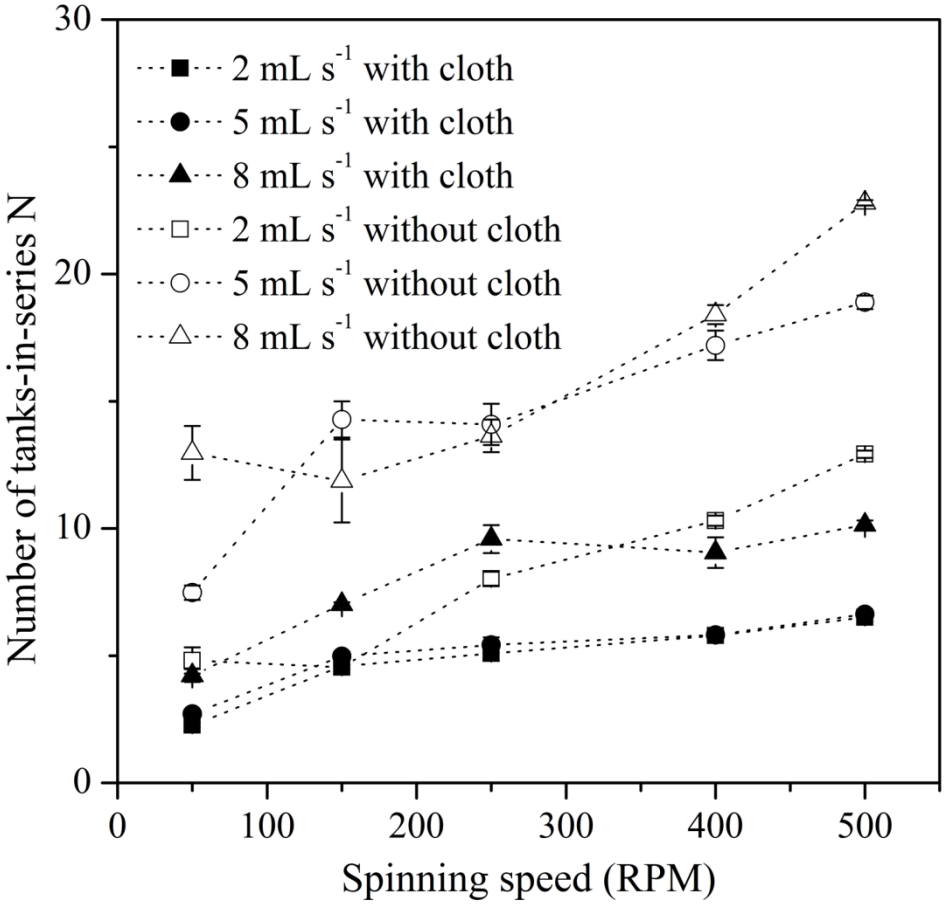

Figure 4

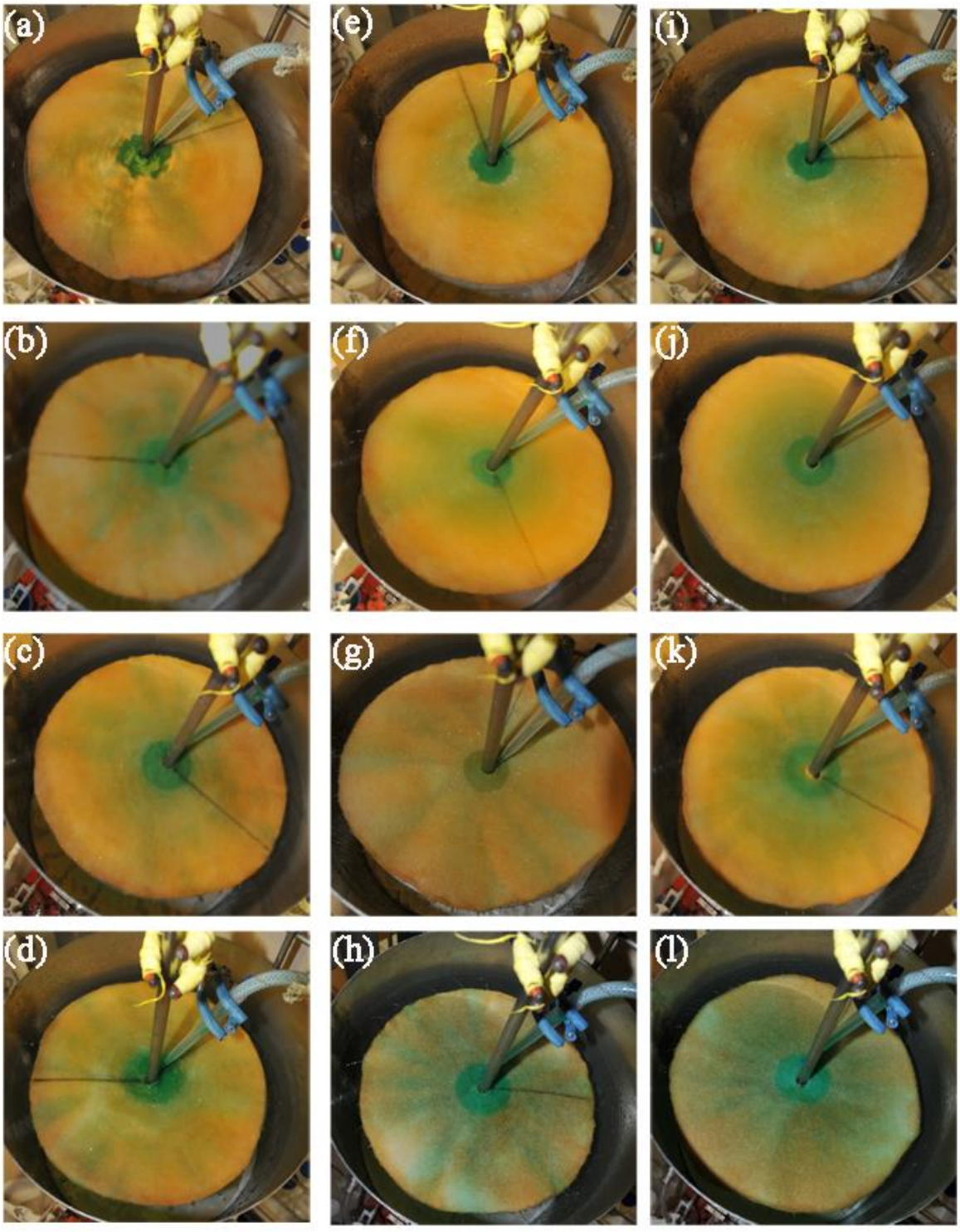

Figure 5

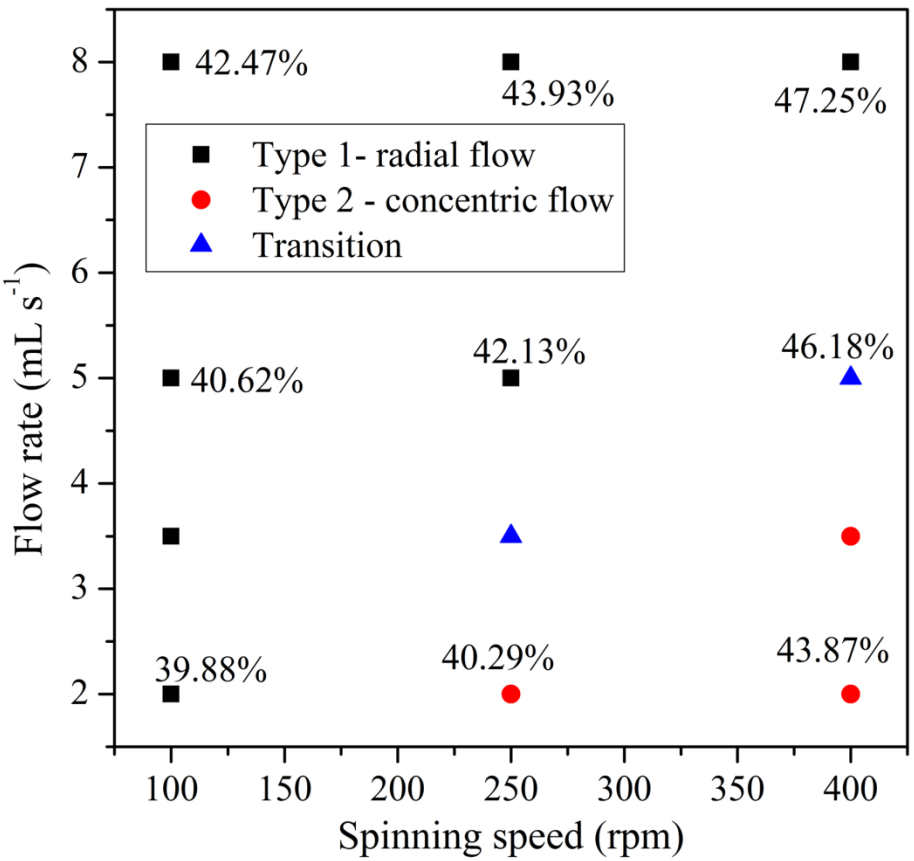

Figure 6

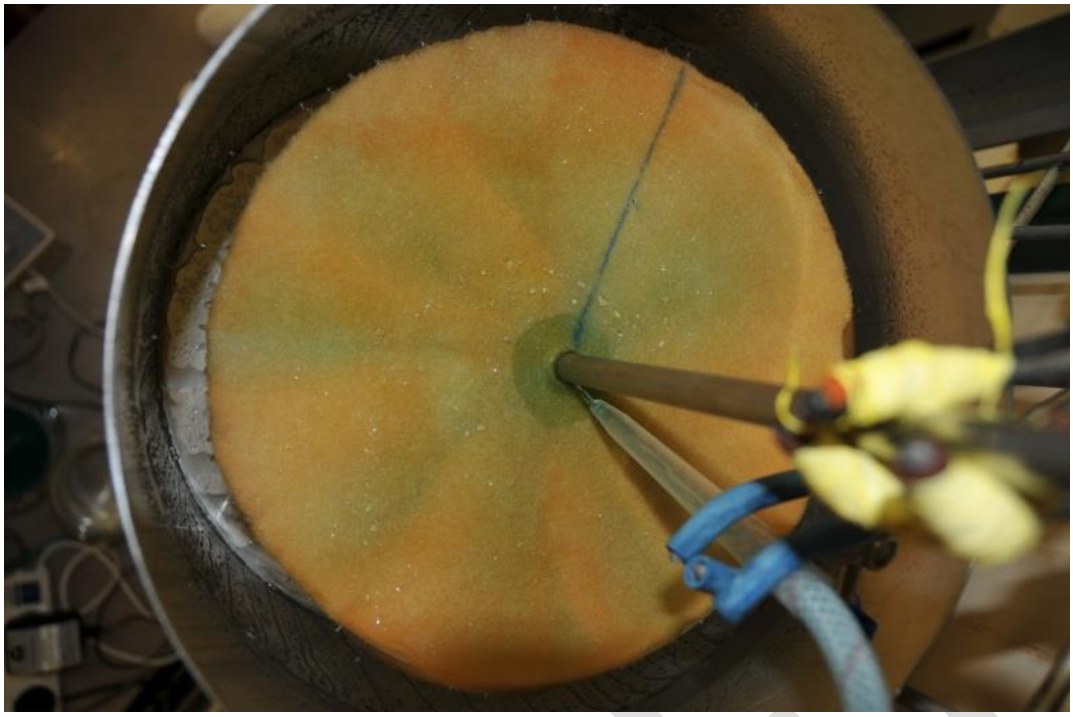

Figure 7

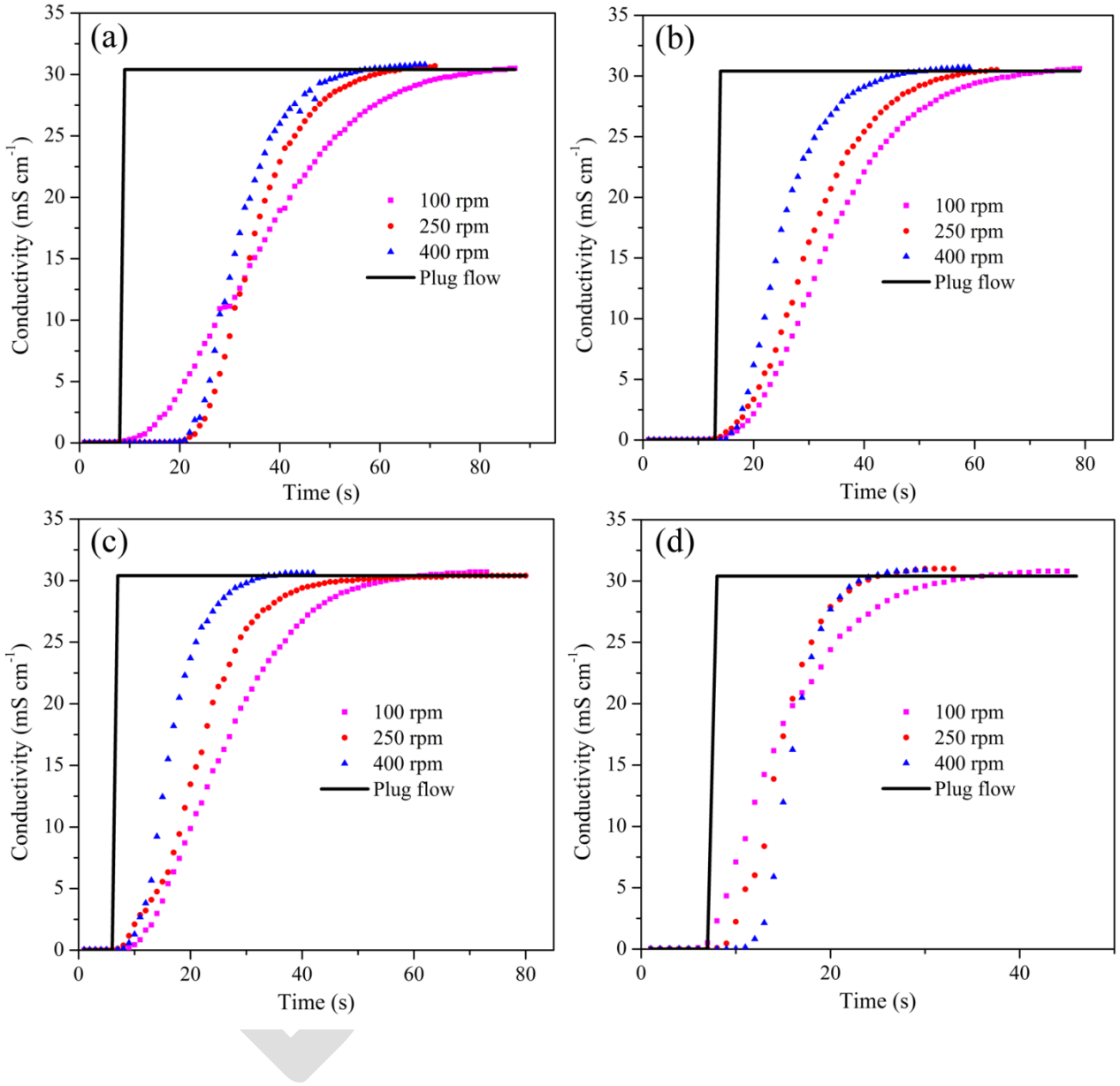
(a)
(b)
(c)
(d)
Conductivity (mS cm^{-1})
Time (s)
100 rpm
250 rpm
400 rpm
Plug flow

Figure 8

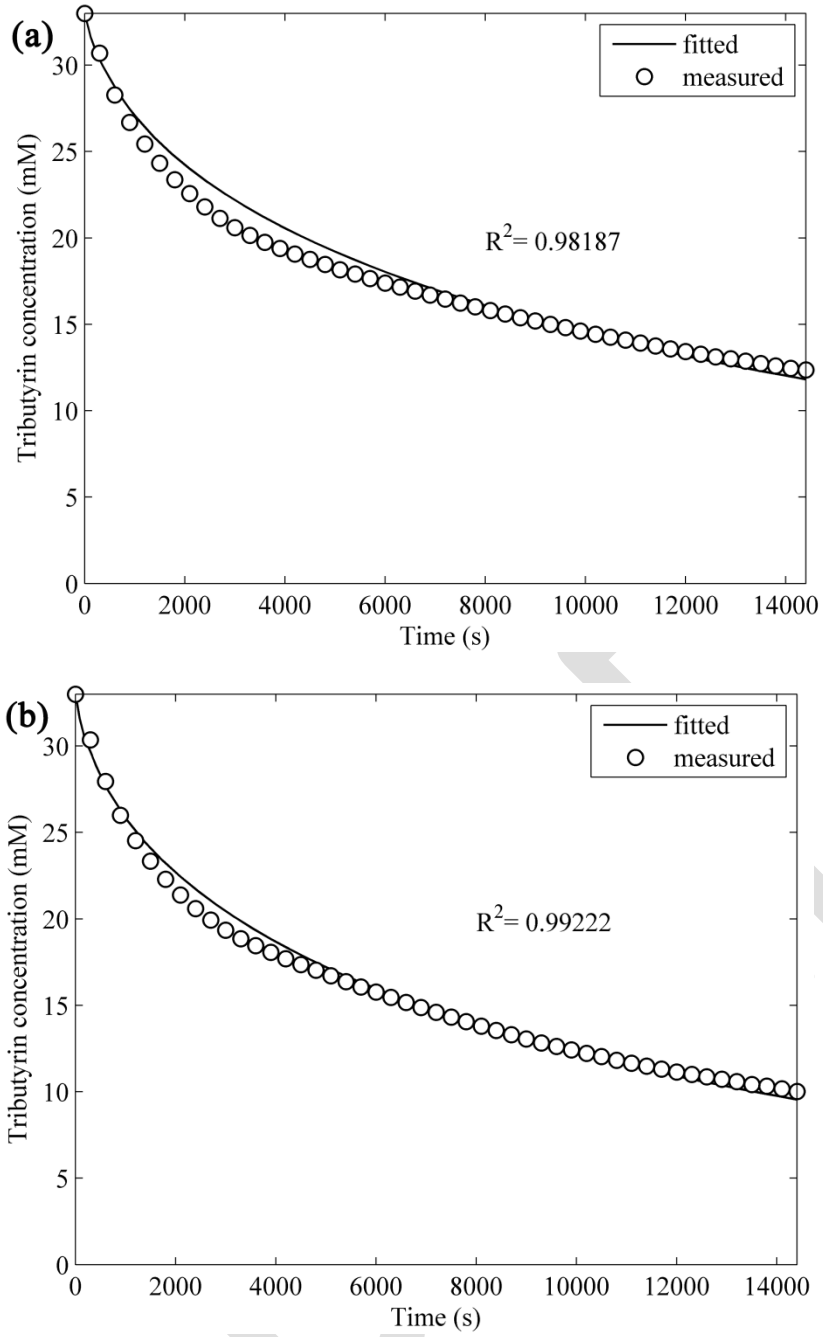
(a)
fitted
measured
R^2= 0.98187
Tributyrin concentration (mM)
Time (s)
0
5
10
15
20
25
30
0
2000
4000
6000
8000
10000
12000
14000
(b)
fitted
measured
R^2= 0.99222
Tributyrin concentration (mM)
Time (s)
0
5
10
15
20
25
30
0
2000
4000
6000
8000
10000
12000
14000

Figure 9

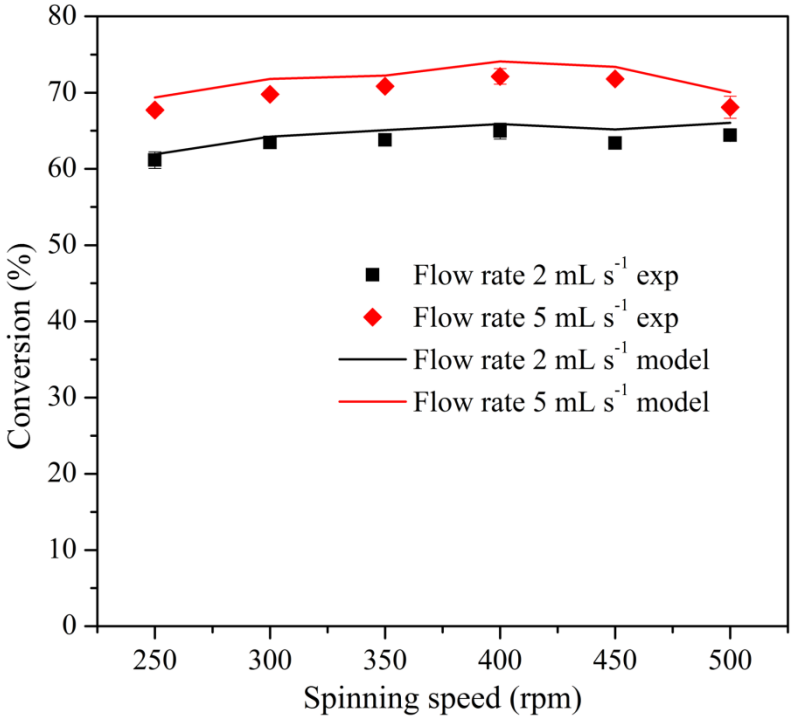

Figure 10

Table 1 Global mass transfer coefficient (s^{-1}) at various spinning speeds and flow rates.

Spinning speed (rpm)	250	300	350	400	450	500
2 mL s^{-1}	0.614	0.670	0.771	0.928	1.097	1.331
5 mL s^{-1}	0.769	0.812	0.952	1.142	1.310	1.462